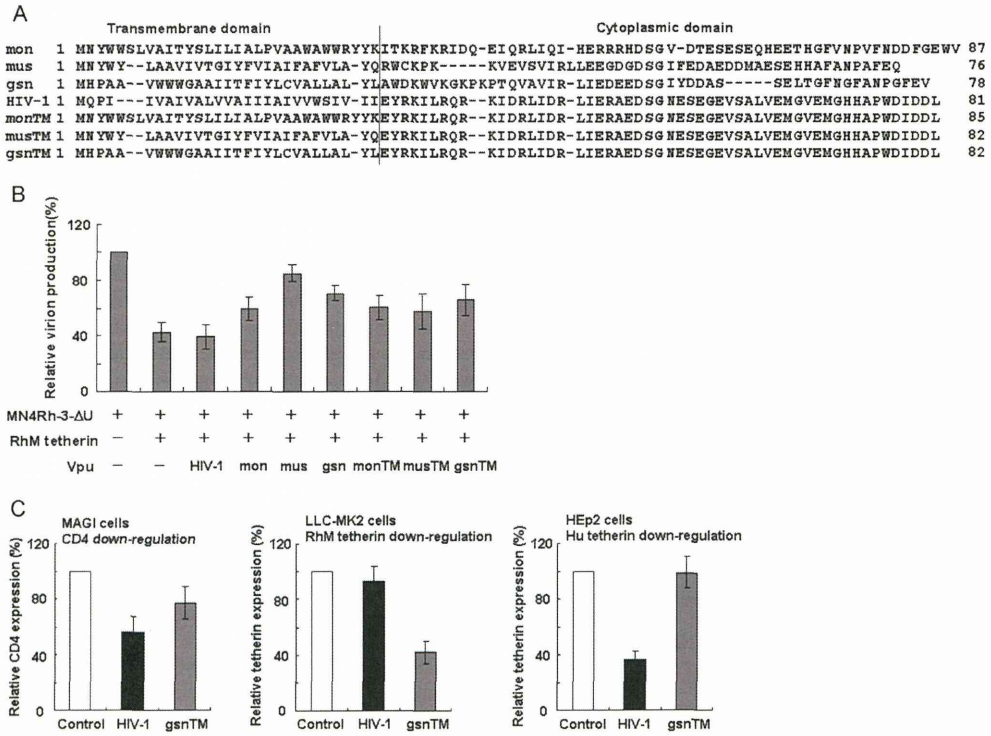

FIG 6 Generation of SIV/HIV-1 chimeric Vpu proteins resistant to macaque tetherin. (A) Amino acid sequences of various Vpu proteins. Alignments of the sequences and the boundary between TM/cytoplasmic domains are shown based on previously reported information (26). mon, SIVmonCML1 (GenBank accession number AY340701); mus, SIVmus1085 (GenBank accession number AY340700); gsn, SIVgsn166 (GenBank accession number AF468659); HIV-1, NL4-3 (32). HIV-1mt clones (MN4 series) have *vpu* genes identical to that of NL4-3. monTM-, musTM-, and gsnTM-Vpu were constructed by fusing each TM domain of SIVmon/mus/gsn Vpu with the cytoplasmic domain of HIV-1_{NL4-3} Vpu. (B) RhM tetherin antagonism by various Vpu proteins. 293T cells were cotransfected with a *vpu*-deficient proviral clone (MN4Rh-3-ΔU), pCIneo-RhM tetherin, and various pSG-VpucFLAG constructs. On day 2 posttransfection, virion production in the culture supernatants was determined by RT assays. Virion production levels relative to that of MN4Rh-3-ΔU in the absence of RhM tetherin were calculated, and mean values of three independent experiments are shown with the standard deviations. (C) Downregulation of cell surface CD4 and tetherin by HIV-1_{NL4-3} Vpu or gsnTM-Vpu. MAGI, LLC-MK2, and HEp2 cells were used to determine the downregulation of CD4, RhM tetherin, and human (Hu) tetherin by Vpu, respectively. Cells were transfected with the pIRES-hrGFP (control), pIRES-HIV-1 Vpu-hrGFP, or pIRES-gsnTM-Vpu-hrGFP construct. On day 2 posttransfection, cells were stained for cell surface CD4 or tetherin and analyzed by two-color flow cytometry. Values presented are CD4 or tetherin fluorescence intensities of GFP-positive cells relative to that of the control. Mean values ± standard deviations of three independent experiments are shown.

central lines of the helices are similar between MN4/LSDQ and MN4/LSDQdtu, whereas they are different in MN4/LSDQgtu. These results suggest the possibility that the structural properties of the tetherin interaction surface of the MN4/LSDQgtu Vpu TM domain are very different from those of the Vpu TM domains of MN4/LSDQ and MN4/LSDQdtu. Further studies are necessary to verify this issue.

RhM APOBEC3-, TRIM5α-, and tetherin-resistant HIV-1mt clone MN4/LSDQgtu replicates comparably to SIVmac239 in RhM PBMCs. Here we constructed distinct HIV-1mt clones with respect to their resistance to RhM TRIM5α and tetherin: TRIM5α- and tetherin-susceptible MN4Rh-3, TRIM5α-resistant but tetherin-susceptible MN4/LSDQ, and TRIM5α- and tetherin-resistant MN4/LSDQgtu. Of note, all these clones are RhM APOBEC3 resistant (see Fig. 1 for their genomes). To investigate the effect of the increased resistance to these macaque restriction factors, various viruses were examined for their growth potential in PBMCs from four *TRIM5α* homozygous RhM individuals. As shown in Fig. 8, SIVmac239, a comparative standard virus in macaque cells, replicated constantly in all PBMC preparations. The growth potentials in the RhM PBMCs of the HIV-1mt clones tested markedly and stably differed. As a likely result of RhM TRIM5α-resistant Gag-CA, MN4/LSDQ replicated much more efficiently than MN4Rh-3. By virtue of RhM tetherin-resistant Vpu, MN4/LSDQgtu grew significantly better than MN4/LSDQ. Essentially the same results for HIV-1mt growth kinetics were obtained in M1.3S cells. The M1.3S cell line and macaque PBMCs always responded similarly to various SIVs/HIVs (our unpublished observations). Moreover, by comparing the peak day of viral growth kinetics and the peak level itself, MN4/LSDQgtu was shown here to have the ability to replicate comparably to SIVmac239 in RhM PBMCs, except for one preparation (from monkey 565) (Fig. 8). The results show that the increased resistance to macaque restriction factors correlates well with the enhanced viral growth potential. In sum, MN4/LSDQgtu, which exhibits resistance to known major restriction factors (APOBEC3, TRIM5, and tetherin

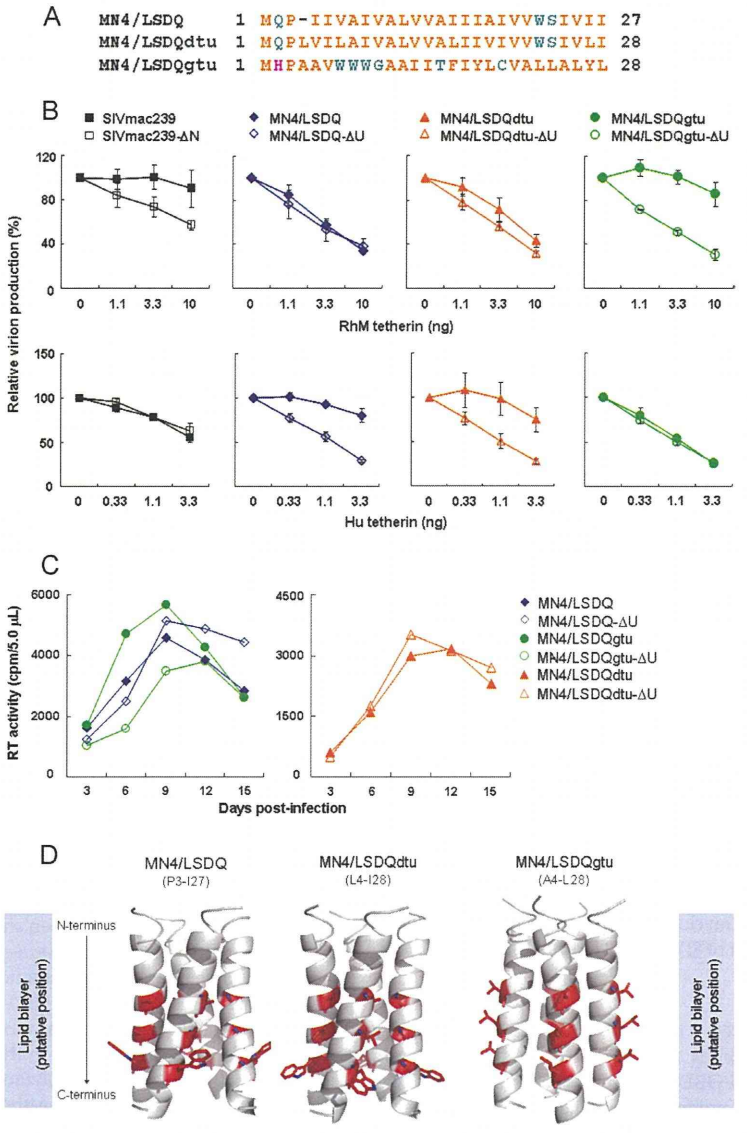

FIG 7 Effects of various Vpu proteins carrying a different TM domain on tetherin antagonism and HIV-1mt replication in macaque cells. (A) Alignment of amino acid sequences of the Vpu TM domain in each HIV-1mt clone. MN4/LSDQ, MN4/LSDQdtu, and MN4/LSDQgtu encode the Vpu TM domain derived from HIV-1_{NL4-3} (32), HIV-1_{DH12} (22), and SIVgsn166 (GenBank accession number AF468659), respectively. (B) Species-specific tetherin antagonism by SIVmac239 and various HIV-1mt clones carrying different Vpu proteins. SIVmac239 (MA239N) and its *nef*-deficient clone (MA239N-ΔN) were used as positive controls for RhM tetherin resistance. 293T cells were cotransfected with proviral clones and the indicated amounts of the pCIneo-RhM tetherin or pCIneo-Human tetherin expression vector. On day 2 posttransfection, virion production was determined by RT activity released into the culture supernatants. Values are presented as RT activity of each sample relative to that of each proviral clone without tetherin expression. Mean values ± standard deviations of three independent experiments are shown. ΔU, *vpu* deficient; Hu, human. (C) Growth kinetics of various HIV-1mt clones and their *vpu*-deficient clones in M1.3S cells. Viruses were prepared from 293T cells transfected with the indicated proviral clones, and equal amounts (5×10^5 RT units) were inoculated into M1.3S cells (2×10^5 cells). Virus replication was monitored by RT activity released into the culture supernatants. Representative data from three independent experiments are shown. (D) Structural modeling of Vpu TM domains of MN4/LSDQ, MN4/LSDQdtu, and MN4/LSDQgtu. Predicted models are shown in a ribbon representation. Amino acid residues corresponding to the residues in HIV-1 Vpu crucial for binding with human tetherin (54) are highlighted in a red stick representation. Crucial residues in Vpu TM domains of MN4/LSDQ, MN4/LSDQdtu, and MN4/LSDQgtu are A14/A18/W22, A15/V19/W23, and T15/L19/L23, respectively. TM regions analyzed (see panel A for amino acid sequences) are indicated in parentheses.

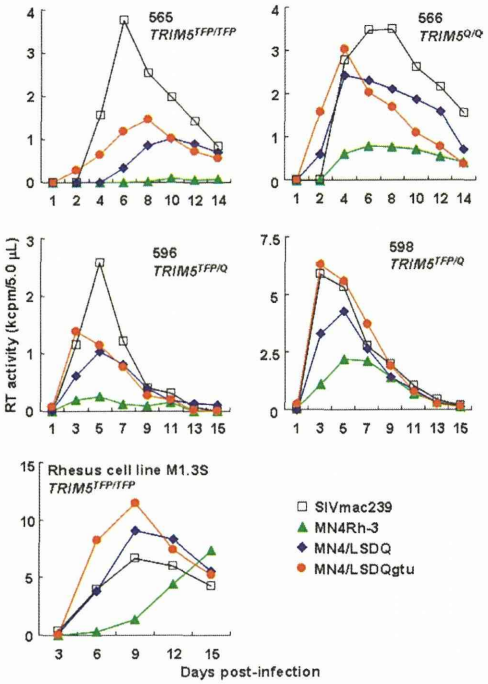

FIG 8 Growth kinetics of SIVmac239 and various HIV-1mt clones in *TRIM5α* homozygous RhM PBMCs. PBMCs were prepared from four RhM individuals with the different *TRIM5* alleles indicated. Viruses were prepared from 293T cells transfected with the indicated proviral clones, and equal amounts (2.5×10^6 RT units) were used to spin infect PBMCs (2×10^6 cells). As a control experiment, rhesus M1.3S cells (2×10^5) were infected with equal amounts of viruses (5×10^5 RT units). Virus replication was monitored by RT activity released into the culture supernatants. Monkey identification numbers are indicated in each panel.

proteins), is the best HIV-1mt clone generated so far, replicating with an efficiency similar to that of SIVmac239 in RhM cells.

DISCUSSION

In this study, we generated a novel HIV-1mt clone, designated MN4/LSDQgtu, that exhibits resistance to RhM TRIM5α and tetherin in addition to APOBEC3 proteins (Fig. 1). By sequence homology- and structure-guided CA mutagenesis and by screening the multicycle growth potential of CA mutant viruses in M1.3S cells, we successfully obtained viruses with enhanced replication efficiency in macaque cells as well as increased macaque TRIM5α resistance (Fig. 2 to 5). The transfer of the TM domain of SIVgsn166 Vpu into the corresponding region of HIV-1mt Vpu conferred the ability to specifically counteract macaque tetherin on the virus (Fig. 6 and 7). Furthermore, the increased resistance to both RhM TRIM5α and tetherin contributed to the viral growth enhancement in RhM PBMCs (Fig. 8).

During the preparation of this paper, McCarthy et al. reported several key residues in SIVmac239 CA involved in the interaction with RhM TRIM5α by genetic and structural analysis (55). Interestingly, the HIV-1mt CA amino acid residues identified in this study as being the elements responsible for the increased resistance to RhM TRIM5α (M94L/R98S/Q110D/G114Q) were included in those residues. McCarthy et al. reported that H4/5L and helix 6 of SIVmac239 CA also affect TRIM5α sensitivity (55). In the construction process for our HIV-1mt clones, we found that the CA elements involved in the interaction with RhM TRIM5α are the CypA-binding loop within H4/5L, H6/7L, M94L/R98S within H4/5L, and Q110D/G114Q in helix 6 (18–20, 56; this study). Of the substitutions identified in this study, R98S was the primary residue to increase TRIM5α resistance and improve viral growth in macaque cells. It was also shown that the TRIM5α ($TRIM5^{TFP}$)-susceptible SIVsmE543-3 clone acquires an adaptive R97S change in CA (corresponding to R98S in MN4Rh-3 CA) to evade TRIM5α ($TRIM5^{TFP}$) restriction during viral replication in RhM individuals (40). In TRIM5α-sensitive CA, R98S may be a key residue contributing to the evasion of TRIM5α restriction. Together, these results suggest that CA elements critical for recognition by TRIM5α may be conserved among primate lentiviruses. The RhM TRIM5α-resistant HIV-1 CA constructed in this study would be useful to define how TRIM5α recognizes CA. On the other hand, MN4/LSDQ appeared not to evade TRIM5α restriction completely, as SIVmac239 did (Fig. 4). In this regard, since it has been shown that the N-terminal β-hairpin domain in the retroviral CA contributes to circumventing TRIM5α (36, 55, 57), we constructed various HIV-1mt clones carrying mutations in the domain (Table 1). However, except for the L6I substitution, none of the clones were infectious (Table 1). A further CA modification(s) may be necessary for complete evasion of TRIM5α restriction.

Accumulating evidence has shown that tetherin is an important cellular restriction factor that affects the replication, adaptation, and evolution of primate immunodeficiency viruses (4, 26). Its negative effect on viral replication is certainly observed in cultured cell lines and primary cells but is not so evident relative to those of APOBEC3 and TRIM5 proteins (10). Also, in the present study, RhM tetherin-resistant Vpu significantly contributed to viral growth enhancement but not as much as TRIM5α-resistant CA (Fig. 7 and 8). However, tetherin has been suggested to play an important effector role in antiretroviral activity induced by alpha interferon (58–60). Also, it has been shown that the pathogenic revertant virus from nonpathogenic *nef*-deficient virus acquires tetherin antagonism by adaptive mutations in the gp41 subunit of Env (61). Therefore, the ability of HIV-1mt clones to antagonize RhM tetherin may be very important for optimal replication and pathogenesis in RhM individuals. In this regard, it has been described that naturally occurring polymorphisms in RhM tetherin sequences are present (30, 31, 61). Although whether these variations have some appreciable effects on viral replication *in vitro* is undetermined, the relationship between tetherin polymorphisms and the viral replication level *in vivo* (animals)/viral pathogenic activity *in vivo* may be a major issue to address and remains to be extensively analyzed. It would be intriguing to elucidate how the viral accessory protein Vpu *in vitro* is associated with the *in vivo* replicative and pathogenic properties of HIV-1 (22).

We constructed an MN4/LSDQgtu clone resistant to the known major restriction factors (APOBEC3, TRIM5, and tetherin proteins) in RhM cells. The growth potential of MN4/LSDQgtu was similar to that of SIVmac239 in most RhM PBMC preparations (Fig. 8). It was shown previously that the *in vivo* replication of SIV is predictable from the virus susceptibility of PBMCs (62, 63). Also, in a series of our studies, the better our HIV-1mt clones grew in PBMCs, the better they grew in the monkeys (20, 24, 64).

Thus, it is expected that MN4/LSDQgtu will grow much better in RhM individuals, at least in the early infection phase, than the other HIV-1mt clones constructed. As reported previously, the replication of HIV-1 derivatives in infected macaques was eventually controlled, and no disease was induced in the animals (16, 20, 21, 24, 64). It has been suggested that the replication ability of primate lentiviruses in unusual hosts is more severely affected, via an interferon-induced antiviral state mediated by unidentified species-specific factors, than that in natural hosts (23). Moreover, there are the other significant issues to be considered, such as viral coreceptor tropism (CXCR4 versus CCR5), the diversity in viral growth properties (HIV-1 versus SIVmac), and the difference in host immune responses (human versus RhM) (9, 65–67). Most importantly, CCR5-tropic but not CXCR4-tropic clones have been found to be appropriate as input viruses to experimentally infect RhMs for various HIV-1 model studies *in vivo* (65–67). Although MN4/LSDQgtu is a CXCR4-tropic virus, it has clear potential for the establishment of a model system. MN4/LSDQgtu can be changed to a pathogenic CCR5-tropic virus through *in vitro* and *in vivo* approaches, as well documented by previous SHIV studies (68–70). It is also possible to generate entirely new CCR5-tropic HIV-1mt clones other than MN4/LSDQgtu derivatives on the basis of the key findings for Gag-CA and Vpu-TM in this study.

Our study here describes the generation and characterization of a novel HIV-1 derivative minimally chimeric with SIVs. Several infection model systems using distinct viruses and nonhuman primates are now available. It is important to define common and unique characteristics of each virus-host interaction based on the results obtained from various experimental approaches, including SIV/natural host and SIVmac/RhM, SHIV/RhM, and HIV-1mt/RhM infection systems. Such efforts would shed light on a better understanding of HIV-1/human infection and HIV-1 pathogenesis.

ACKNOWLEDGMENTS

This study was supported in part by a grant from the Ministry of Health, Labor and Welfare of Japan (Research on HIV/AIDS project no. H23-003).

We thank Kazuko Yoshida for editorial assistance.

We declare that no competing interests exist.

REFERENCES

1. **Kirchhoff F.** 2010. Immune evasion and counteraction of restriction factors by HIV-1 and other primate lentiviruses. Cell Host Microbe **8**:55–67.
2. **Sharp PM, Hahn BH.** 2011. Origins of HIV and the AIDS pandemic. Cold Spring Harb. Perspect. Med. 1:a006841. doi:10.1101/cshperspect.a006841.
3. **Shibata R, Sakai H, Kawamura M, Tokunaga K, Adachi A.** 1995. Early replication block of human immunodeficiency virus type 1 in monkey cells. J. Gen. Virol. **76**:2723–2730.
4. **Blanco-Melo D, Venkatesh S, Bieniasz PD.** 2012. Intrinsic cellular defenses against human immunodeficiency viruses. Immunity **37**:399–411.
5. **Harris RS, Hultquist JF, Evans DT.** 2012. The restriction factors of human immunodeficiency virus. J. Biol. Chem. **287**:40875–40883.
6. **Malim MH, Bieniasz PD.** 2012. HIV restriction factors and mechanisms of evasion. Cold Spring Harb. Perspect. Med. **2**:a006940. doi:10.1101/cshperspect.a006940.
7. **Hatziioannou T, Evans DT.** 2012. Animal models for HIV/AIDS research. Nat. Rev. Microbiol. **10**:852–867.
8. **Nomaguchi M, Doi N, Fujiwara S, Adachi A.** 2011. Macaque-tropic HIV-1 derivatives: a novel experimental approach to understand viral replication and evolution *in vivo*, p 325–348. *In* Chang T.Y.-L. (ed), HIV-host interactions. InTech, Rijeka, Croatia. http://www.intechopen.com/books/hiv-host-interactions/macaque-tropic-hiv-1-derivatives-a-novel-experimental-approach-to-understand-viral-replication-and-e.
9. **Shedlock DJ, Silvestri G, Weiner DB.** 2009. Monkeying around with HIV vaccines: using rhesus macaques to define 'gatekeepers' for clinical trials. Nat. Rev. Immunol. **9**:717–728.
10. **Nomaguchi M, Doi N, Matsumoto Y, Sakai Y, Fujiwara S, Adachi A.** 2012. Species tropism of HIV-1 modulated by viral accessory proteins. Front. Microbiol. **3**:267. doi:10.3389/fmicb.2012.00267.
11. **Holmes RK, Malim MH, Bishop KN.** 2007. APOBEC-mediated viral restriction: not simply editing? Trends Biochem. Sci. **32**:118–128.
12. **Malim MH, Emerman M.** 2008. HIV-1 accessory proteins—ensuring viral survival in a hostile environment. Cell Host Microbe **3**:388–398.
13. **Grütter MG, Luban J.** 2012. TRIM5 structure, HIV-1 capsid recognition, and innate immune signaling. Curr. Opin. Virol. **2**:142–150.
14. **Nakayama EE, Shioda T.** 2010. Anti-retroviral activity of TRIM5 alpha. Rev. Med. Virol. **20**:77–92.
15. **Douglas JL, Gustin JK, Viswanathan K, Mansouri M, Moses AV, Früh K.** 2010. The great escape: viral strategies to counter BST-2/tetherin. PLoS Pathog. **6**:e1000913. doi:10.1371/journal.ppat.1000913.
16. **Hatziioannou T, Ambrose Z, Chung NP, Piatak M, Jr, Yuan F, Trubey CM, Coalter V, Kiser R, Schneider D, Smedley J, Pung R, Gathuka M, Estes JD, Veazey RS, KewalRamani VN, Lifson JD, Bieniasz PD.** 2009. A macaque model of HIV-1 infection. Proc. Natl. Acad. Sci. U. S. A. **106**:4425–4429.
17. **Hatziioannou T, Princiotta M, Piatak M, Jr, Yuan F, Zhang F, Lifson JD, Bieniasz PD.** 2006. Generation of simian-tropic HIV-1 by restriction factor evasion. Science **314**:95. doi:10.1126/science.1130994.
18. **Kamada K, Igarashi T, Martin MA, Khamsri B, Hatcho K, Yamashita T, Fujita M, Uchiyama T, Adachi A.** 2006. Generation of HIV-1 derivatives that productively infect macaque monkey lymphoid cells. Proc. Natl. Acad. Sci. U. S. A. **103**:16959–16964.
19. **Nomaguchi M, Yokoyama M, Kono K, Nakayama EE, Shioda T, Saito A, Akari H, Yasutomi Y, Matano T, Sato H, Adachi A.** 2013. Gag-CA Q110D mutation elicits TRIM5-independent enhancement of HIV-1mt replication in macaque cells. Microbes Infect. **15**:56–65.
20. **Saito A, Nomaguchi M, Iijima S, Kuroishi A, Yoshida T, Lee YJ, Hayakawa T, Kono K, Nakayama EE, Shioda T, Yasutomi Y, Adachi A, Matano T, Akari H.** 2011. Improved capacity of a monkey-tropic HIV-1 derivative to replicate in cynomolgus monkeys with minimal modifications. Microbes Infect. **13**:58–64.
21. **Thippeshappa R, Polacino P, Yu Kimata MT, Siwak EB, Anderson D, Wang W, Sherwood L, Arora R, Wen M, Zhou P, Hu SL, Kimata JT.** 2011. Vif substitution enables persistent infection of pig-tailed macaques by human immunodeficiency virus type 1. J. Virol. **85**:3767–3779.
22. **Shingai M, Yoshida T, Martin MA, Strebel K.** 2011. Some human immunodeficiency virus type 1 Vpu proteins are able to antagonize macaque BST-2 *in vitro* and *in vivo*: Vpu-negative simian-human immunodeficiency viruses are attenuated *in vivo*. J. Virol. **85**:9708–9715.
23. **Bitzegeio J, Sampias M, Bieniasz PD, Hatziioannou T.** 2013. Adaptation to the interferon-induced antiviral state by human and simian immunodeficiency viruses. J. Virol. **87**:3549–3560.
24. **Saito A, Nomaguchi M, Kono K, Iwatani Y, Yokoyama M, Yasutomi Y, Sato H, Shioda T, Sugiura W, Matano T, Adachi A, Nakayama E, Akari H.** 2013. *TRIM5* genotypes in cynomolgus monkeys primarily influence inter-individual diversity in susceptibility to monkey-tropic human immunodeficiency virus type 1. J. Gen. Virol. **94**:1318–1324.
25. **Doi N, Fujiwara S, Adachi A, Nomaguchi M.** 2011. Rhesus M1.3S cells suitable for biological evaluation of macaque-tropic HIV/SIV clones. Front. Microbiol. **2**:115. doi:10.3389/fmicb.2011.00115.
26. **Sauter D, Schindler M, Specht A, Landford WN, Münch J, Kim KA, Votteler J, Schubert U, Bibollet-Ruche F, Keele BF, Takehisa J, Ogando Y, Ochsenbauer C, Kappes JC, Ayouba A, Peeters M, Learn GH, Shaw G, Sharp PM, Bieniasz P, Hahn BH, Hatziioannou T, Kirchhoff F.** 2009. Tetherin-driven adaptation of Vpu and Nef function and the evolution of pandemic and nonpandemic HIV-1 strains. Cell Host Microbe **6**:409–421.
27. **Lebkowski JS, Clancy S, Calos MP.** 1985. Simian virus 40 replication in adenovirus-transformed human cells antagonizes gene expression. Nature **317**:169–171.
28. **Kimpton J, Emerman M.** 1992. Detection of replication-competent and pseudotyped human immunodeficiency virus with a sensitive cell line on the basis of activation of an integrated beta-galactosidase gene. J. Virol. **66**:2232–2239.
29. **Nomaguchi M, Doi N, Fujiwara S, Fujita M, Adachi A.** 2010. Site-

directed mutagenesis of HIV-1 *vpu* gene demonstrates two clusters of replication-defective mutants with distinct ability to down-modulate cell surface CD4 and tetherin. Front. Microbiol. 1:116. doi:10.3389/fmicb.2010.00116.
30. **McNatt MW, Zang T, Hatziioannou T, Bartlett M, Fofana IB, Johnson WE, Neil SJ, Bieniasz PD.** 2009. Species-specific activity of HIV-1 Vpu and positive selection of tetherin transmembrane domain variants. PLoS Pathog. 5:e1000300. doi:10.1371/journal.ppat.1000300.
31. **Yoshida T, Kao S, Strebel K.** 2011. Identification of residues in the BST-2 TM domain important for antagonism by HIV-1 Vpu using a gain-of-function approach. Front. Microbiol. 2:35. doi:10.3389/fmicb.2011.00035.
32. **Adachi A, Gendelman HE, Koenig S, Folks T, Willey R, Rabson A, Martin MA.** 1986. Production of acquired immunodeficiency syndrome-associated retrovirus in human and nonhuman cells transfected with an infectious molecular clone. J. Virol. 59:284–291.
33. **Willey RL, Smith DH, Lasky LA, Theodore TS, Earl PL, Moss B, Capon DJ, Martin MA.** 1988. In vitro mutagenesis identifies a region within the envelope gene of the human immunodeficiency virus that is critical for infectivity. J. Virol. 62:139–147.
34. **O'Doherty U, Swiggard WJ, Malim MH.** 2000. Human immunodeficiency virus type 1 spinoculation enhances infection through virus binding. J. Virol. 74:10074–10080.
35. **Wilson SJ, Webb BL, Ylinen LM, Verschoor E, Heeney JL, Towers GJ.** 2008. Independent evolution of an antiviral TRIMCyp in rhesus macaques. Proc. Natl. Acad. Sci. U. S. A. 105:3557–3562.
36. **Kono K, Song H, Yokoyama M, Sato H, Shioda T, Nakayama EE.** 2010. Multiple sites in the N-terminal half of simian immunodeficiency virus capsid protein contribute to evasion from rhesus monkey TRIM5α-mediated restriction. Retrovirology 7:72. doi:10.1186/1742-4690-7-72.
37. **Howard BR, Vajdos FF, Li S, Sundquist WI, Hill CP.** 2003. Structural insights into the catalytic mechanism of cyclophilin A. Nat. Struct. Biol. 10:475–481.
38. **Park SH, Mrse AA, Nevzorov AA, Mesleh MF, Oblatt-Montal M, Montal M, Opella SJ.** 2003. Three-dimensional structure of the channel-forming trans-membrane domain of virus protein "u" (Vpu) from HIV-1. J. Mol. Biol. 333:409–424.
39. **Leaver-Fay A, Tyka M, Lewis SM, Lange OF, Thompson J, Jacak R, Kaufman K, Renfrew PD, Smith CA, Sheffler W, Davis IW, Cooper S, Treuille A, Mandell DJ, Richter F, Ban YE, Fleishman SJ, Corn JE, Kim DE, Lyskov S, Berrondo M, Mentzer S, Popović Z, Havranek JJ, Karanicolas J, Das R, Meiler J, Kortemme T, Gray JJ, Kuhlman B, Baker D, Bradley P.** 2011. ROSETTA3: an object-oriented software suite for the simulation and design of macromolecules. Methods Enzymol. 487:545–574.
40. **Kirmaier A, Wu F, Newman RM, Hall LR, Morgan JS, O'Connor S, Marx PA, Meythaler M, Goldstein S, Buckler-White A, Kaur A, Hirsch VM, Johnson WE.** 2010. *TRIM5* suppresses cross-species transmission of a primate immunodeficiency virus and selects for emergence of resistant variants in the new species. PLoS Biol. 8:e1000462. doi:10.1371/journal.pbio.1000462.
41. **Newman RM, Hall L, Connole M, Chen GL, Sato S, Yuste E, Diehl W, Hunter E, Kaur A, Miller GM, Johnson WE.** 2006. Balancing selection and the evolution of functional polymorphism in Old World monkey TRIM5alpha. Proc. Natl. Acad. Sci. U. S. A. 103:19134–19139.
42. **Price AJ, Marzetta F, Lammers M, Ylinen LM, Schaller T, Wilson SJ, Towers GJ, James LC.** 2009. Active site remodeling switches HIV specificity of antiretroviral TRIMCyp. Nat. Struct. Mol. Biol. 16:1036–1042.
43. **Ylinen LM, Price AJ, Rasaiyaah J, Hué S, Rose NJ, Marzetta F, James LC, Towers GJ.** 2010. Conformational adaptation of Asian macaque TRIMCyp directs lineage specific antiviral activity. PLoS Pathog. 6:e1001062. doi:10.1371/journal.ppat.1001062.
44. **Fassati A.** 2012. Multiple roles of the capsid protein in the early steps of HIV-1 infection. Virus Res. 170:15–24.
45. **Ganser-Pornillos BK, Yeager M, Sundquist WI.** 2008. The structural biology of HIV assembly. Curr. Opin. Struct. Biol. 18:203–217.
46. **Miyamoto T, Yokoyama M, Kono K, Shioda T, Sato H, Nakayama EE.** 2011. A single amino acid of human immunodeficiency virus type 2 capsid protein affects conformation of two external loops and viral sensitivity to TRIM5α. PLoS One 6:e22779. doi:10.1371/journal.pone.0022779.
47. **Nomaguchi M, Doi N, Fujiwara S, Saito A, Akari H, Nakayama EE, Shioda T, Yokoyama M, Sato H, Adachi A.** 2013. Systemic biological analysis of the mutations in two distinct HIV-1mt genomes occurred during replication in macaque cells. Microbes Infect. 15:319–328.
48. **Hatziioannou T, Cowan S, Von Schwedler UK, Sundquist WI, Bieniasz PD.** 2004. Species-specific tropism determinants in the human immunodeficiency virus type 1 capsid. J. Virol. 78:6005–6012.
49. **Owens CM, Song B, Perron MJ, Yang PC, Stremlau M, Sodroski J.** 2004. Binding and susceptibility to postentry restriction factors in monkey cells are specified by distinct regions of the human immunodeficiency virus type 1 capsid. J. Virol. 78:5423–5437.
50. **von Schwedler UK, Stray KM, Garrus JE, Sundquist WI.** 2003. Functional surfaces of the human immunodeficiency virus type 1 capsid protein. J. Virol. 77:5439–5450.
51. **Lim SY, Rogers T, Chan T, Whitney JB, Kim J, Sodroski J, Letvin NL.** 2010. TRIM5alpha modulates immunodeficiency virus control in rhesus monkeys. PLoS Pathog. 6:e1000738. doi:10.1371/journal.ppat.1000738.
52. **Jia B, Serra-Moreno R, Neidermyer W, Rahmberg A, Mackey J, Fofana IB, Johnson WE, Westmoreland S, Evans DT.** 2009. Species-specific activity of SIV Nef and HIV-1 Vpu in overcoming restriction by tetherin/BST2. PLoS Pathog. 5:e1000429. doi:10.1371/journal.ppat.1000429.
53. **Zhang F, Wilson SJ, Landford WC, Virgen B, Gregory D, Johnson MC, Munch J, Kirchhoff F, Bieniasz PD, Hatziioannou T.** 2009. Nef proteins from simian immunodeficiency viruses are tetherin antagonists. Cell Host Microbe 6:54–67.
54. **Vigan R, Neil SJ.** 2010. Determinants of tetherin antagonism in the transmembrane domain of the human immunodeficiency virus type 1 Vpu protein. J. Virol. 84:12958–12970.
55. **McCarthy KR, Schmidt AG, Kirmaier A, Wyand AL, Newman RM, Johnson WE.** 2013. Gain-of-sensitivity mutations in a Trim5-resistant primary isolate of pathogenic SIV identify two independent conserved determinants of Trim5α specificity. PLoS Pathog. 9:e1003352. doi:10.1371/journal.ppat.1003352.
56. **Kuroishi A, Saito A, Shingai Y, Shioda T, Nomaguchi M, Adachi A, Akari H, Nakayama EE.** 2009. Modification of a loop sequence between alpha-helices 6 and 7 of virus capsid (CA) protein in a human immunodeficiency virus type 1 (HIV-1) derivative that has simian immunodeficiency virus (SIVmac239) vif and CA alpha-helices 4 and 5 loop improves replication in cynomolgus monkey cells. Retrovirology 6:70. doi:10.1186/1742-4690-6-70.
57. **Ohkura S, Goldstone DC, Yap MW, Holden-Dye K, Taylor IA, Stoye JP.** 2011. Novel escape mutants suggest an extensive TRIM5α binding site spanning the entire outer surface of the murine leukemia virus capsid protein. PLoS Pathog. 7:e1002011. doi:10.1371/journal.ppat.1002011.
58. **Homann S, Smith D, Little S, Richman D, Guatelli J.** 2011. Upregulation of BST-2/tetherin by HIV infection *in vivo*. J. Virol. 85:10659–10668.
59. **Liberatore RA, Bieniasz PD.** 2011. Tetherin is a key effector of the antiretroviral activity of type I interferon in vitro and in vivo. Proc. Natl. Acad. Sci. U. S. A. 108:18097–18101.
60. **Pillai SK, Abdel-Mohsen M, Guatelli J, Skasko M, Monto A, Fujimoto K, Yukl S, Greene WC, Kovari H, Rauch A, Fellay J, Battegay M, Hirschel B, Witteck A, Bernasconi E, Ledergerber B, Günthard HF, Wong JK, Swiss HIV Cohort Study.** 2012. Role of retroviral restriction factors in the interferon-α-mediated suppression of HIV-1 in vivo. Proc. Natl. Acad. Sci. U. S. A. 109:3035–3040.
61. **Serra-Moreno R, Jia B, Breed M, Alvarez X, Evans DT.** 2011. Compensatory changes in the cytoplasmic tail of gp41 confer resistance to tetherin/BST-2 in a pathogenic nef-deleted SIV. Cell Host Microbe 9:46–57.
62. **Goldstein S, Brown CR, Dehghani H, Lifson JD, Hirsch VM.** 2000. Intrinsic susceptibility of rhesus macaque peripheral CD4(+) T cells to simian immunodeficiency virus in vitro is predictive of in vivo viral replication. J. Virol. 74:9388–9395.
63. **Lifson JD, Nowak MA, Goldstein S, Rossio JL, Kinter A, Vasquez G, Wiltrout TA, Brown C, Schneider D, Wahl L, Lloyd AL, Williams J, Elkins WR, Fauci AS, Hirsch VM.** 1997. The extent of early viral replication is a critical determinant of the natural history of simian immunodeficiency virus infection. J. Virol. 71:9508–9514.
64. **Igarashi T, Iyengar R, Byrum RA, Buckler-White A, Dewar RL, Buckler CE, Lane HC, Kamada K, Adachi A, Martin MA.** 2007. Human immunodeficiency virus type 1 derivative with 7% simian immunodeficiency virus genetic content is able to establish infections in pig-tailed macaques. J. Virol. 81:11549–11552.
65. **Lifson JD, Haigwood NL.** 2012. Lessons in nonhuman primate models for AIDS vaccine research: from minefields to milestones. Cold Spring Harb. Perspect. Med. 2:a007310. doi:10.1101/cshperspect.a007310.
66. **Shaw GM, Hunter E.** 2012. HIV transmission. Cold Spring Harb. Perspect. Med. 2:a006965. doi:10.1101/cshperspect.a006965.

67. **Swanstrom R, Coffin J.** 2012. HIV-1 pathogenesis: the virus. Cold Spring Harb. Perspect. Med. **2**:a007443. doi:10.1101/cshperspect.a007443.
68. **Nishimura Y, Shingai M, Willey R, Sadjadpour R, Lee WR, Brown CR, Brenchley JM, Buckler-White A, Petros R, Eckhaus M, Hoffman V, Igarashi T, Martin MA.** 2010. Generation of the pathogenic R5-tropic simian/human immunodeficiency virus $SHIV_{AD8}$ by serial passaging in rhesus macaques. J. Virol. **84**:4769–4781.
69. **Ren W, Mumbauer A, Gettie A, Seaman MS, Russell-Lodrigue K, Blanchard J, Westmoreland S, Cheng-Mayer C.** 2013. Generation of lineage-related, mucosally transmissible subtype C R5 simian-human immunodeficiency viruses capable of AIDS development, induction of neurological disease, and coreceptor switching in rhesus macaques. J. Virol. **87**:6137–6149.
70. **Shingai M, Donau OK, Schmidt SD, Gautam R, Plishka RJ, Buckler-White A, Sadjadpour R, Lee WR, LaBranche CC, Montefiori DC, Mascola JR, Nishimura Y, Martin MA.** 2012. Most rhesus macaques infected with the CCR5-tropic $SHIV_{AD8}$ generate cross-reactive antibodies that neutralize multiple HIV-1 strains. Proc. Natl. Acad. Sci. U. S. A. **109**:19769–19774.
71. **Shibata R, Kawamura M, Sakai H, Hayami M, Ishimoto A, Adachi A.** 1991. Generation of a chimeric human and simian immunodeficiency virus infectious to monkey peripheral blood mononuclear cells. J. Virol. **65**:3514–3520.
72. **Kawamura M, Sakai H, Adachi A.** 1994. Human immunodeficiency virus Vpx is required for the early phase of replication in peripheral blood mononuclear cells. Microbiol. Immunol. **38**:871–878.
73. **Gamble TR, Vajdos FF, Yoo S, Worthylake DK, Houseweart M, Sundquist WI, Hill CP.** 1996. Crystal structure of human cyclophilin A bound to the amino-terminal domain of HIV-1 capsid. Cell **87**:1285–1294.

ARTICLES
PUBLISHED ONLINE: 24 NOVEMBER 2013 | DOI: 10.1038/NCHEM.1795
nature chemistry

Oligomerization transforms human APOBEC3G from an efficient enzyme to a slowly dissociating nucleic acid-binding protein

Kathy R. Chaurasiya[1], Micah J. McCauley[1], Wei Wang[2], Dominic F. Qualley[2], Tiyun Wu[3], Shingo Kitamura[4], Hylkje Geertsema[1], Denise S. B. Chan[5], Amber Hertz[3], Yasumasa Iwatani[3,4], Judith G. Levin[3], Karin Musier-Forsyth[2], Ioulia Rouzina[6] and Mark C. Williams[1]*

The human APOBEC3 proteins are a family of DNA-editing enzymes that play an important role in the innate immune response against retroviruses and retrotransposons. APOBEC3G is a member of this family that inhibits HIV-1 replication in the absence of the viral infectivity factor Vif. Inhibition of HIV replication occurs by both deamination of viral single-stranded DNA and a deamination-independent mechanism. Efficient deamination requires rapid binding to and dissociation from ssDNA. However, a relatively slow dissociation rate is required for the proposed deaminase-independent roadblock mechanism in which APOBEC3G binds the viral template strand and blocks reverse transcriptase-catalysed DNA elongation. Here, we show that APOBEC3G initially binds ssDNA with rapid on–off rates and subsequently converts to a slowly dissociating mode. In contrast, an oligomerization-deficient APOBEC3G mutant did not exhibit a slow off rate. We propose that catalytically active monomers or dimers slowly oligomerize on the viral genome and inhibit reverse transcription.

APOBEC3 proteins are DNA-editing enzymes that are part of the innate human immune response to viral pathogens, including retroviruses and retrotransposons[1–4]. Of all the A3 proteins, A3G[5] is the most potent inhibitor of HIV-1 replication[1,4,6], reducing viral infectivity by several orders of magnitude in the absence of the HIV-1 viral infectivity factor Vif[7–9]. In fact, the function of Vif is to specifically counteract the antiviral activity of A3G[1,9].

Although A3G is the most studied of all the APOBEC proteins, the molecular mechanism for A3G-mediated HIV-1 restriction is still not fully understood. A3G is a deoxycytidine deaminase, which converts deoxycytidine bases in single-stranded DNA (ssDNA) to deoxyuridine[5,10–14]. A3G deamination of minus-strand viral DNA formed during reverse transcription results in G to A hypermutation in the plus-strand[11,12,15], which effectively impairs viral replication. However, there are several lines of evidence that suggest that a deaminase-independent mechanism is also involved[1,6,16]. First, A3G catalytic mutants retain antiviral activity[17–20]. Second, A3G inhibits hepatitis B virus replication without G to A hypermutation[21]. Third, A3A inhibits LINE-1 and Alu retrotransposition[22–28] and parvovirus replication[24,29] independent of deaminase activity. Further evidence for a non-editing mechanism is based on the reduction of minus-strand viral DNA levels in HIV-1 particles during endogenous reverse transcription[30], inhibition of reverse transcriptase (RT)-catalysed viral DNA elongation *in vitro* by catalytic A3G mutants[31,32], inhibition of strand transfer reactions *in vitro* and in cell-based assays[32–34], and A3G-induced inhibition of reverse transcription in viruses from human $CD4^+$ T cells[35]. A roadblock model—in which A3G molecules bind the template strand at one or a few locations and physically block viral DNA synthesis—has therefore been proposed as a molecular mechanism for deaminase-independent inhibition[32].

Because only 7 ($\pm$4) A3G molecules are incorporated into each *vif*-deficient virion[36], RT inhibition by an A3G roadblock requires a slow A3G off rate from single-stranded nucleic acids. In contrast, these few A3G molecules must have fast on–off rates to deaminate up to 1,000 sites in several minutes[14] using a rapid search mechanism on viral ssDNA[37,38]. To resolve this apparent paradox, we hypothesize that A3G exhibits fast binding kinetics as a monomer or dimer in order to function as an efficient enzyme, and slow kinetics on oligomerization in order to block RT from elongating viral DNA. To test this idea, we used optical tweezers to monitor A3G binding kinetics on a single DNA molecule.

Results

Single-molecule measurements of A3G binding to ssDNA. For these studies, a single double-stranded λ-DNA molecule was tethered to two polystyrene beads, with one bead held in an optical trap and another on a micropipette tip. As the fixed bead was gradually moved away from the optically trapped bead, the force on the DNA molecule was measured at each extension, yielding a force–extension curve (Fig. 1, solid black line). The solution surrounding the single DNA molecule can be exchanged to measure the effects of DNA-binding ligands on the properties of DNA.

In the absence of binding ligands, force-induced melting occurs at a constant force of 61.0 $\pm$ 0.5 pN, generating ssDNA, either by

[1]Department of Physics, Northeastern University, Boston, Massachusetts 02115, USA, [2]Department of Chemistry and Biochemistry, Center for Retrovirus Research, and Center for RNA Biology, The Ohio State University, Columbus, Ohio 43210, USA, [3]Section on Viral Gene Regulation, Program on Genomics of Differentiation, Eunice Kennedy Shriver National Institute of Child Health and Human Development, National Institutes of Health, Bethesda, Maryland 20892, USA, [4]Clinical Research Center, National Hospital Organization Nagoya Medical Center, Nagoya, Aichi 460-0001, Japan, [5]Department of Structural Biology, University of Pittsburgh School of Medicine, Pittsburgh, Pennsylvania 15260, USA, [6]Department of Biochemistry, Molecular Biology and Biophysics, University of Minnesota, Minneapolis, Minnesota 55455, USA. *e-mail: mark@neu.edu

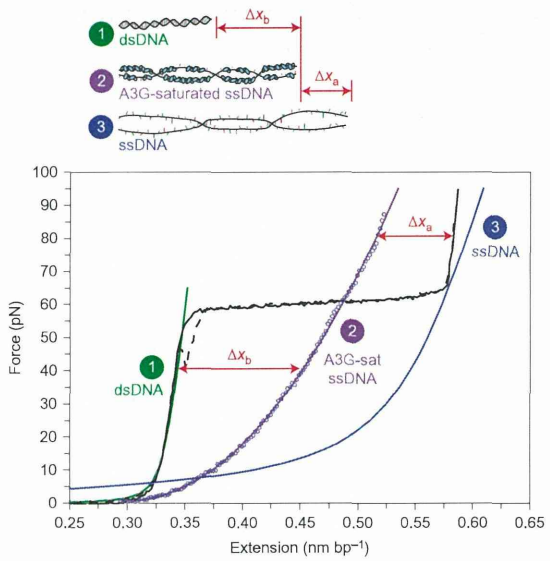

Figure 1 | Force-dependent difference in length between DNA and a saturated A3G–DNA complex allows us to measure A3G binding. Typical extension in nm per base pair (bp) (solid black) and return (dashed black line) of a single DNA molecule. At 61.0 ± 0.5 pN, the molecule undergoes a force-induced melting transition from dsDNA (green line, Supplementary equation (1)) to ssDNA (blue line). A3G-saturated ssDNA (200 nM A3G, $t > 500$ s, data points fit to Supplementary equation (4), solid purple line) is longer than dsDNA (Δx_b, below the melting transition) and shorter than ssDNA (Δx_a, above the melting transition). A3G-saturated ssDNA is significantly shorter than ssDNA only (blue line, Supplementary equation (2)), which suggests that A3G may wrap ssDNA on binding.

peeling from the ends or by forming melting bubbles[39]. Although a stretched form of dsDNA called S-DNA may form on overstretching at monovalent salt concentrations above 150 mM, it is well-established that overstretching is force-induced melting in the presence of ssDNA binding proteins and at the ionic strength of 50 mM used in this work[39,40]. At the end of the overstretching transition, the bead movement reverses direction and the DNA tension is gradually released (Fig. 1, dashed black line). The minimal hysteresis, or mismatch between DNA extension and release, indicates that the ssDNA generated by force reanneals immediately into dsDNA during the return. At any given point along the transition, the molecule is a well-characterized combination of dsDNA and ssDNA (Supplementary equation (3))[40]. Pausing at fixed extension during the melting transition allows precise control of the fraction of ssDNA substrate available for protein binding.

The force–extension curve probes the length of the captured DNA molecule at a given force. At forces above 7 pN, ssDNA is longer than dsDNA. We exploit this force-dependent difference in length to measure the ssDNA binding properties of A3G. A3G-saturated ssDNA, obtained at a high protein concentration by first overstretching the DNA and then allowing A3G to fully bind and stabilize the DNA in its single-stranded form, is longer than dsDNA and shorter than ssDNA (Fig. 1). Accordingly, A3G bound to ssDNA increases the molecule length by Δx_b when below the melting transition, and reduces it by Δx_a when above the melting transition.

In the presence of 50 nM A3G, the extension curve follows the DNA-only curve before the melting transition, reflecting no measurable binding to dsDNA (Fig. 2a, solid line). A3G only binds after force-induced melting generates ssDNA. Based on the observed hysteresis (Fig. 2a, dashed line), most of the protein does not dissociate on DNA release, preventing the two strands from fully reannealing. A3G-bound ssDNA is longer than dsDNA (Fig. 1), so the change in length at a given force (Fig. 2a, Δx_t) describes the total fraction of A3G bound to ssDNA (f_{total}; Supplementary Fig. 1a).

A second stretch of the same molecule does not retrace the release curve, revealing that some fraction of the protein has dissociated during the 30 s incubation at zero force between stretch–release cycles (Fig. 2b). As soon as any A3G dissociates at forces below the force-induced melting transition, the two strands reanneal into dsDNA, which is shorter than A3G-bound ssDNA (Fig. 2b, Δx_f). Accordingly, the second stretch reflects the fraction of A3G that remains ssDNA-bound (f_{slow}), which allows the fraction that dissociates quickly (f_{fast}) to be quantified as $f_{fast} = f_{total} - f_{slow}$. The DNA was held at zero force for 30 s between the first release and the second stretch, but longer wait times of up to 120 min do not lead to further measurable dissociation (data not shown).

In this experiment, A3G was exposed to ssDNA for 50 s. However, A3G oligomerization observed in bulk experiments occurs on much longer timescales[37]. To measure slow binding, A3G was incubated for 250 s with ssDNA generated by force-induced melting (Fig. 2c). The DNA release curve obtained after this incubation exhibits a length increase relative to the initial release curve (Fig. 2c, Δx_i), because additional A3G binds ssDNA during incubation. This effect increases at longer incubation times (Fig. 2d), approaching the A3G-saturated ssDNA curve (Fig. 1). Fits to the DNA release curves at increasing incubation time yield $f_{total}(t)$, while the subsequent stretch (data not shown) quantifies $f_{slow}(t)$, and $f_{fast}(t)$ is the difference between the two. These measurements for 50 nM A3G are presented in Fig. 3a.

Quantitative binding model. The slow binding component increases at the expense of the fast component, suggesting that the A3G-ssDNA reaction may be modelled as a two-step process:

$$\text{A3G} + \text{ssDNA} \underset{k_{-1}}{\overset{k_1 c}{\rightleftharpoons}} (\text{A3G/ssDNA})_{fast} \underset{k_{-2}}{\overset{k_2}{\rightleftharpoons}} (\text{A3G/ssDNA})_{slow} \quad (1)$$

in which an initial bimolecular process leads to a fast complex that converts to a slow, more stable complex in the second unimolecular step. Binding rates were obtained from fits to this model (Supplementary equations (9)–(11)) at five A3G concentrations (Fig. 3b). (A3G precipitates at high concentrations[19], so experiments were calibrated using force–extension curves at known protein concentrations.) As expected, the observed fast rate k_{fast} and the on rate $k_1 c$ are both linear with A3G concentration (Fig. 3c). The bimolecular rate constant $k_1 = 1.5\ (\pm 0.1) \times 10^5\ M^{-1}\ s^{-1}$ and off rate $k_{-1} = 1.2\ (\pm 0.1) \times 10^{-2}\ s^{-1}$ are consistent with single-molecule Förster resonance energy transfer (FRET)[41] and fluorescence spectroscopy[37] measurements, considering differences in solution conditions. The observed slow rate k_{slow} saturates at high A3G concentrations (Fig. 3d), and both the on and off rates for the second, unimolecular step are concentration-independent ($k_2 = 6.7\ (\pm 0.6) \times 10^{-3}\ s^{-1}$ and $k_{-2} = 2.8\ (\pm 0.5) \times 10^{-5}\ s^{-1}$). Elementary reaction rates were obtained from the data in several different ways, and agreement of the resulting values (Supplementary Table 2) supports the binding model.

Oligomerization is responsible for slow binding. To determine whether slow binding is due to A3G oligomerization, we expressed and purified the F126A/W127A A3G mutant (A3G FW), which is severely defective in oligomerization[42]. When this mutant was incubated with ssDNA for 1,050 s, the release curve

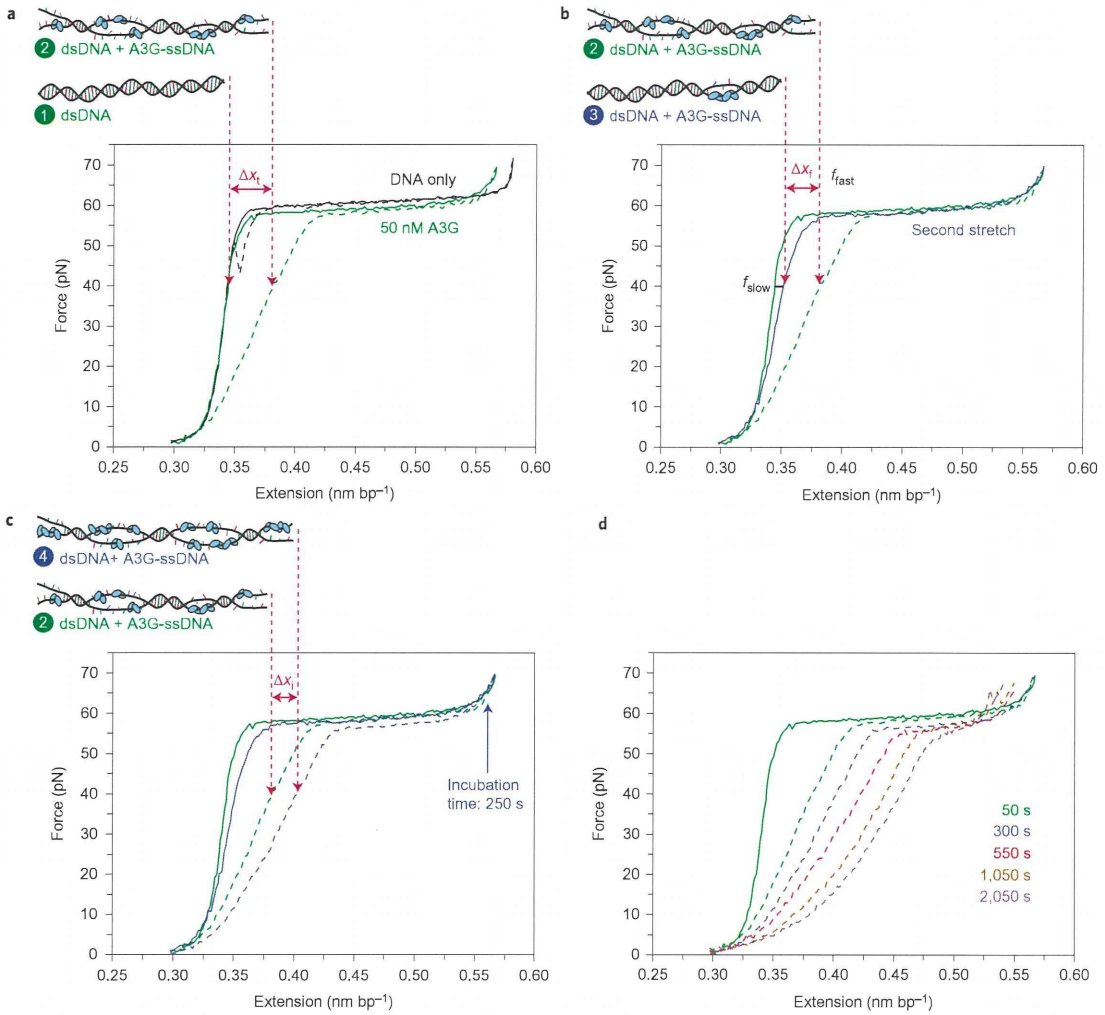

Figure 2 | Single-molecule method to measure fast and slow fractions of A3G binding. a, Without protein (black line), a single DNA molecule reanneals immediately on release, exhibiting minimal hysteresis, or mismatch between stretch (solid) and release (dashed) curves. In the presence of 50 nM A3G, the stretch curve (solid green line) follows the dsDNA-only curve, indicating negligible A3G–dsDNA binding. A3G binds the exposed ssDNA and prohibits the DNA strands from reannealing, resulting in hysteresis (dashed green line). For a given force (40 pN shown), there is a corresponding change in DNA length Δx_t between A3G-free dsDNA (left arrow, drawing 1) and partially A3G-bound ssDNA (right arrow, drawing 2). This force-dependent length change measures A3G–ssDNA binding (Supplementary Fig 1). **b**, The second stretch (solid blue line) lies between the first stretch and release curves, distinguishing the fraction of A3G that remains bound (f_{slow}) from the fraction that dissociated (f_{fast}) before the second stretch. The A3G that dissociates rapidly allows the strands to reanneal immediately into dsDNA (drawing 3), resulting in length decrease Δx_f. **c**, Pausing at fixed DNA extension after incubating ssDNA with 50 nM A3G results in additional binding (drawing 4), indicated by the corresponding length increase Δx_i measured during DNA release. **d**, A3G binding increases with total exposure time to ssDNA (dashed lines).

exhibited minimal hysteresis (Fig. 4a), and all the bound protein dissociated before the subsequent stretch (Fig. 4b). A direct comparison of the hysteresis observed for wild-type and mutant A3G is shown in Fig. 4c. The lack of a slow ssDNA bound fraction observed for the mutant, together with the striking difference between the hysteresis observed for the two proteins, shows that the oligomerization-defective mutant does not exhibit slow ssDNA binding kinetics. We therefore conclude that the slow kinetics observed for wild-type A3G is due to oligomerization.

Discussion

Here, we use a single-molecule method that allows us to quantify two distinct modes of A3G binding to ssDNA and characterize the conversion of a fast state into a slow state. These results suggest a binding mechanism in which monomers or dimers initially bind ssDNA and rapidly reach equilibrium ($1/k_{fast} = 24 \pm 1$ s at 200 nM), before slowly converting to oligomers ($1/k_{slow} = 206 \pm 20$ s) (Fig. 5a). Previous bulk solution experiments have established that A3G oligomerizes in the presence of single-stranded nucleic acids[42,43], which inhibits efficient deaminase activity[42]. We also

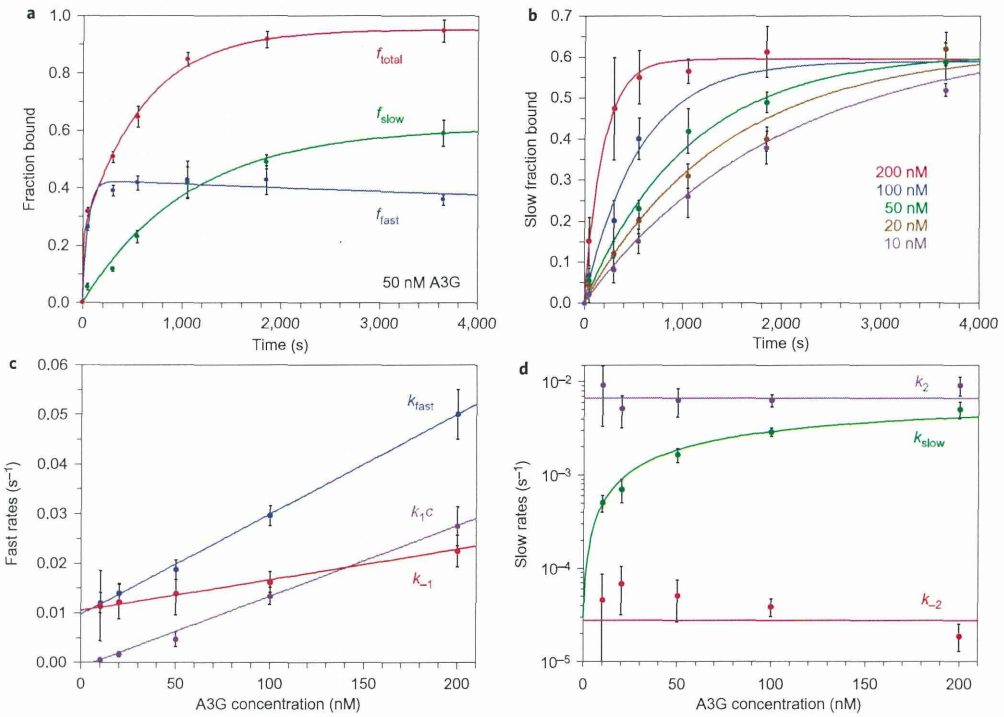

Figure 3 | Quantifying A3G binding reveals association and dissociation rates for fast and slow binding modes. a, Total binding at 50 nM A3G (f_{total}, red) separated into a fast fraction (f_{fast}, blue) and slow fraction (f_{slow}, green), as a function of ssDNA–A3G incubation time. Fits to the binding model (solid lines, Supplementary equations (9)–(11)) yield observed rates k_{fast} and k_{slow}. **b**, Slow fraction bound as a function of time for five A3G concentrations. Solid lines are fits to Supplementary equation (10). Error bars (**a**, **b**) are standard error ($N \geq 3$) for 50–200 nM A3G and propagated error for 10–20 nM A3G. **c**, Fast rates (k_{fast}, blue data points) obtained from fits to the binding model (shown in **a** for 50 nM A3G). The linear fit (solid blue line, Supplementary equation (13)) yields k_1 and k_{-1}. k_1c (purple data points) and k_{-1} (red data points) were also calculated from the binding model. Linear fits (solid lines, Supplementary equations (15) and (17)) yield consistent values of k_1 and k_{-1}. **d**, Slow rates (k_{slow}, green data points) from fits to the binding model (**b**). Fits to Supplementary equation (21) (solid green line, Supplementary Fig. 2b) yield k_2 and k_{-2}. Separate calculations of k_2 (purple) and k_{-2} (red) from the binding model (Supplementary equations (24) and (25)) are also shown. Error bars in **c**,**d** are from uncertainty in the fits to the binding model for total rates k_{fast} and k_{slow}, and propagated error for calculated elementary reaction rates.

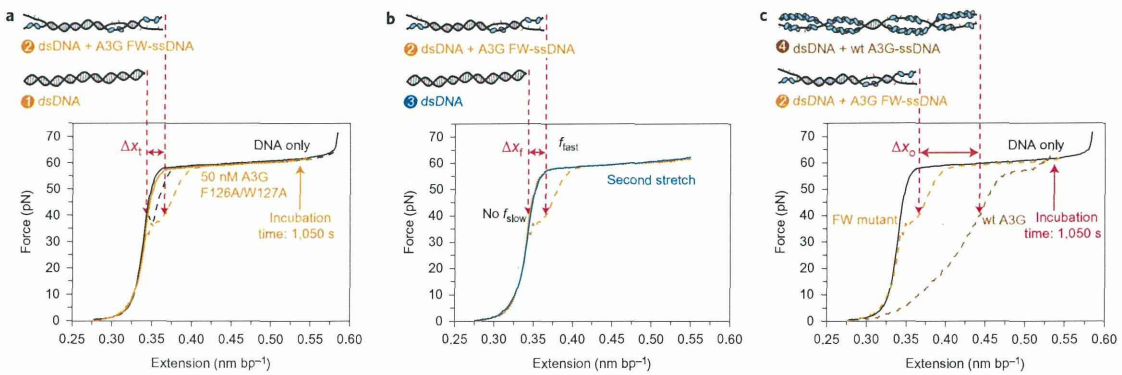

Figure 4 | Oligomerization-defective mutant F126A/W127A (FW) demonstrates that the slow kinetics observed for wild-type A3G is due to oligomerization. a, In the absence of protein (black line), a single DNA molecule reanneals immediately on release, exhibiting minimal hysteresis between extension (solid) and release (dashed). In the presence of 50 nM F126A/W127A A3G (orange line), the stretch curve (solid) follows the dsDNA-only curve, indicating no measurable A3G FW binding to dsDNA (drawing 1). Pausing at fixed DNA extension after the melting transition to incubate the ssDNA with the protein results in ssDNA binding (drawing 2), indicated by the corresponding increase in length Δx_t measured during DNA release at a given force (shown for 40 pN). **b**, The subsequent stretch (dark blue) follows the initial stretch curve (solid orange line), indicating that all the mutant A3G bound during incubation dissociates rapidly (drawing 3), resulting in a decrease in length Δx_f. **c**, Wild-type A3G (drawing 4) exhibits a greater change in length Δx_o relative to the FW mutant (drawing 2) at 1,050 s incubation due to oligomerization on ssDNA.